

Magnetotelluric exploration of deep-seated gold deposits in the Qingchengzi orefield, Eastern Liaoning (China), using a SEP system

Qingyun Di^{a,b,d,e}, Guoqiang Xue^{c,d,e,*}, Qingdong Zeng^{c,d,e}, Zhongxing Wang^{a,b,d,e}, Zhiguo An^{a,b,d,e}, Da lei^{a,b,d,e}

^a Key Laboratory of Shale Gas and Geoengineering, Institute of Geology and Geophysics, Chinese Academy of Sciences, Beijing 100029 China

^b Frontier Technology and Equipment Development Center for Deep Resources Exploration, Institute of Geology and Geophysics, Chinese Academy of Sciences, Beijing 100029, China

^c Key Laboratory of Mineral Resources, Institute of Geology and Geophysics, Chinese Academy of Sciences, Beijing 100029 China

^d College of Earth and Planetary Sciences, University of Chinese Academy of Sciences, Beijing, 100049, China

^e Innovation Academy for Earth Science, Chinese Academy of Sciences, Beijing, 100029, China



ARTICLE INFO

Keywords:

Gold deposits
Liaodong
Surface electromagnetic prospecting system (SEP)
Magnetotellurics
Deep geophysical imaging

ABSTRACT

The Liaodong Peninsula in northern China has undergone multi-stage magmatic and tectonic modifications, similar to those recorded by the Jiaodong gold province that is the largest gold-producing district in China, indicating that Liaodong Peninsula has great potential for new discoveries. However, no significant gold deposit has been discovered thus far at depths below 1.5 km, the typical depth of the gold-bearing system in the comparable Jiaodong gold province. This study focused on the Qingchengzi orefield on the northern Liaodong Peninsula. Qingchengzi recorded multiple post-magmatic hydrothermal gold-mineralizing events along the Jianshanzi fault zone, the main ore-controlling structure in the orefield. Given the potential for undiscovered, deep-seated gold mineralization along the Jianshanzi fault zone, we performed a magnetotelluric (MT) study designed to identify any deeper exploration targets. The surface electromagnetic prospecting (SEP) system, a portable instrument suitable for use in electromagnetically mountain environments, was employed for the purpose of acquiring the MT data. Shallow conductive anomalies identified in the vicinity of the Jianshanzi fault zone were tested by known drilling recorder. The survey not only helped to generate a detailed map of the deep geological architecture, but also allowed us to estimate the vertical extent of the known gold orebody to a depth of more than 2 km.

1. Introduction

In recent years, several gold deposit clusters have been discovered in the eastern North China Craton (NCC) (Mingguo Zhai et al., 2002). One of these clusters, the Liaodong gold province in the eastern NCC, is believed to be genetically related to the destruction of the NCC (Weidong, 2015; Rixiang et al., 2015). Since the 1950s, several medium- to large-type gold-polymetallic deposit clusters (locally addressed as orefields) have been discovered on the Liaodong Peninsula, such as Qingchengzi, Wulong, and Maoling (Fig. 1). Although approximately 300 t Au resources have thus far been discovered in the Liaodong gold province, this endowment is much smaller than that of the Jiaodong gold province, which contains total proven reserves of approximately 4500 t Au. One possible explanation for the large difference in endowment between them may be that Liaodong is poorly

explored at depths greater 1500 m whilst Jiaodong has been explored to depths up to 4060 m (Lianchang Zhang et al., 2018).

Recently, several new gold deposits have been discovered in the Qingchengzi Pb-Zn-Au-Ag orefield of the Liaodong Peninsula (Bin Yu et al., 2018), including Linjiasandaogou (c. 48 t Au at an average grade of 5.2 g/t Au) (Guoping Liu and Yongfu Ai, 2002; Zuquan DU et al., 2008) and Baiyun (c. 34 t Au at an average grade of 2.5 g/t) (Jun Liu et al., 2019). Given these significant discoveries, the Liaodong gold province is conceived to have excellent potential for discovery of additional gold mineralization, especially at depths greater than 1500 m. Therefore, the adoption of new geophysical instruments and methods capable of imaging the deep earth are essential for more effective deep exploration and a key ingredient for realizing future exploration success (Qingdong et al., 2019).

Reliable geophysical instruments are crucial for exploring deeply

* Corresponding author.

E-mail address: ppxueguoqiang@163.com (G. Xue).

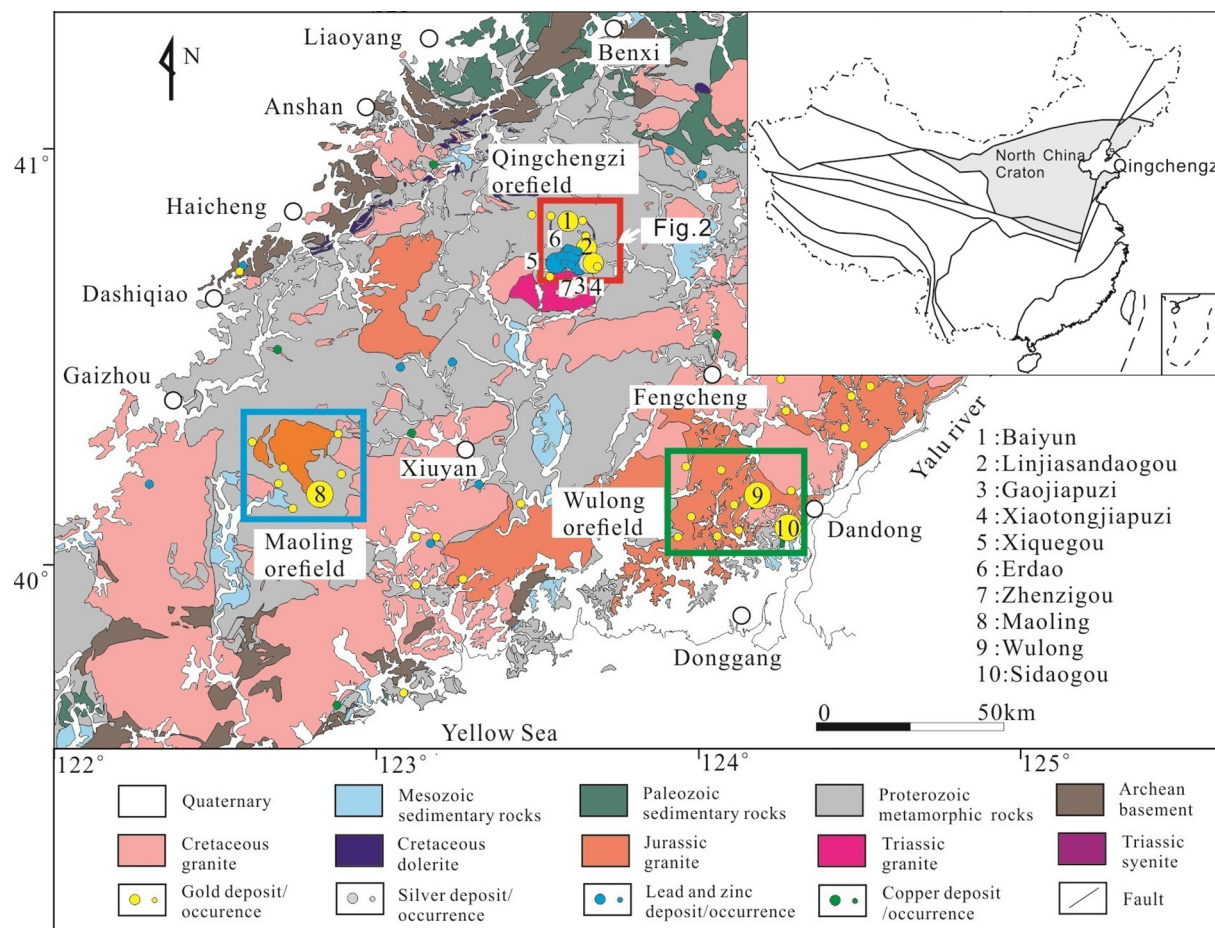


Fig. 1. Geological map of the Liaodong area. The three gold orefields are outlined with solid rectangles. Major gold deposits in the area are marked with solid yellow circles (following Sun et al., 2019b).

concealed mineral resources. Time or frequency domain electromagnetic methods utilized in combination with geophysical instruments include the MTU-RT system developed by Phoenix Geophysics, the GDP-32 multifunction receiver developed by Zonge International, the MT-24 system developed by Electromagnetic Instruments, and the ADU-07 system developed by Metronix Geophysics (Qingyun Di, 2002, 2006). Although those instruments could be used for deep earth geophysical exploration, their effectiveness is reduced in areas characterized by mountainous terrain as is the case for Liaodong. Compact and portable electromagnetic instruments that are lightweight and boost high signal-to-noise ratios are crucial given the aforementioned field conditions on the Liaodong Peninsula. Therefore, we developed a customized surface electromagnetic prospecting (SEP) system able to tackle these issues (Qingyun Di et al., 2012, 2013). A comparative test was of the newly developed technology was previously undertaken and described by Qingyun Di 2015, Qingyun Di et al., 2015.

Whilst the Jianshanzi fault zone (Fig. 2) is known to be gold-mineralized to depths of approximately 420 m it is not known whether the gold orebody has potential to extend deep underground and whether further orebodies may occur within 3000 m depth. Given the difficult mountainous terrain and the fact that the traditional geophysical equipment is heavy (13 kg), the newly developed, portable (3 kg) SEP equipment was used to collect magnetotelluric (MT) data and image the geometry of the Jianshanzi fault zone.

The main aims of this study were to test (1) the newly developed portable SEP system in logistically and electromagnetically challenging terrain and (2) whether the system would be capable of predicting the locations and dimensions of any deep MT anomalies associated with the Jianshanzi fault zone that may represent yet undiscovered, deep-seated

gold ores.

2. Geological setting

The Qingchengzi Pb-Zn-Au-Ag orefield is located in the central part of the Liaodong area. As demonstrated in the Fig. 2, several polymetallic deposits (including Pb-Zn, Ag, Au, and Mo deposits) have been discovered, with a proven reserve of ~300 t Au, 4000 t Ag, and 1.6 Mt Pb-Zn (Yuwang Wang et al., 2017). The basement rocks of the Liaodong Peninsula are composed of the Archean Tonalite-Trondhjemite-Granodiorite (TTG) suite and Paleoproterozoic metavolcanic rocks (BGMELP, 1989).

The Paleoproterozoic Liaohe Group, which unconformably overlies the Archean TTG, is composed of the Gaixian Formation, Dashiqiao Formation, and Langzishan Formation (Fig. 2). The Langzishan Formation is mainly composed of graphite-bearing marble, amphibolite schist, sillimanite-mica schist, and marble. Dolomitic marble, mica-strip marble, granulite-bearing tremolite marble, garnet-mica schist, and sillimanite-mica schist are the most widely distributed rocks in the Dashiqiao Formation. The Gaixian Formation is mainly composed of mica schist, sillimanite-mica schist, garnet-mica schist, and marble-bearing tremolite schist. Multiple intrusions were identified in this area, including the Dadingzi stock, the Shuangdinggou stock, the Xinling stock, the Yaojiagou stock, the northwestward diorite dyke, the northeastward lamprophyre, and the granite porphyry dikes (Fig. 2). The Dadingzi intrusion is composed of monzonite granite with zircon U-Pb age of $1,869 \pm 16$ Ma (Yunhong Wang et al., 2016). The Shuangdinggou intrusion is composed of monzonite granite with zircon U-Pb age of 224.2 ± 1.2 Ma. The Xinling intrusion consists of granite

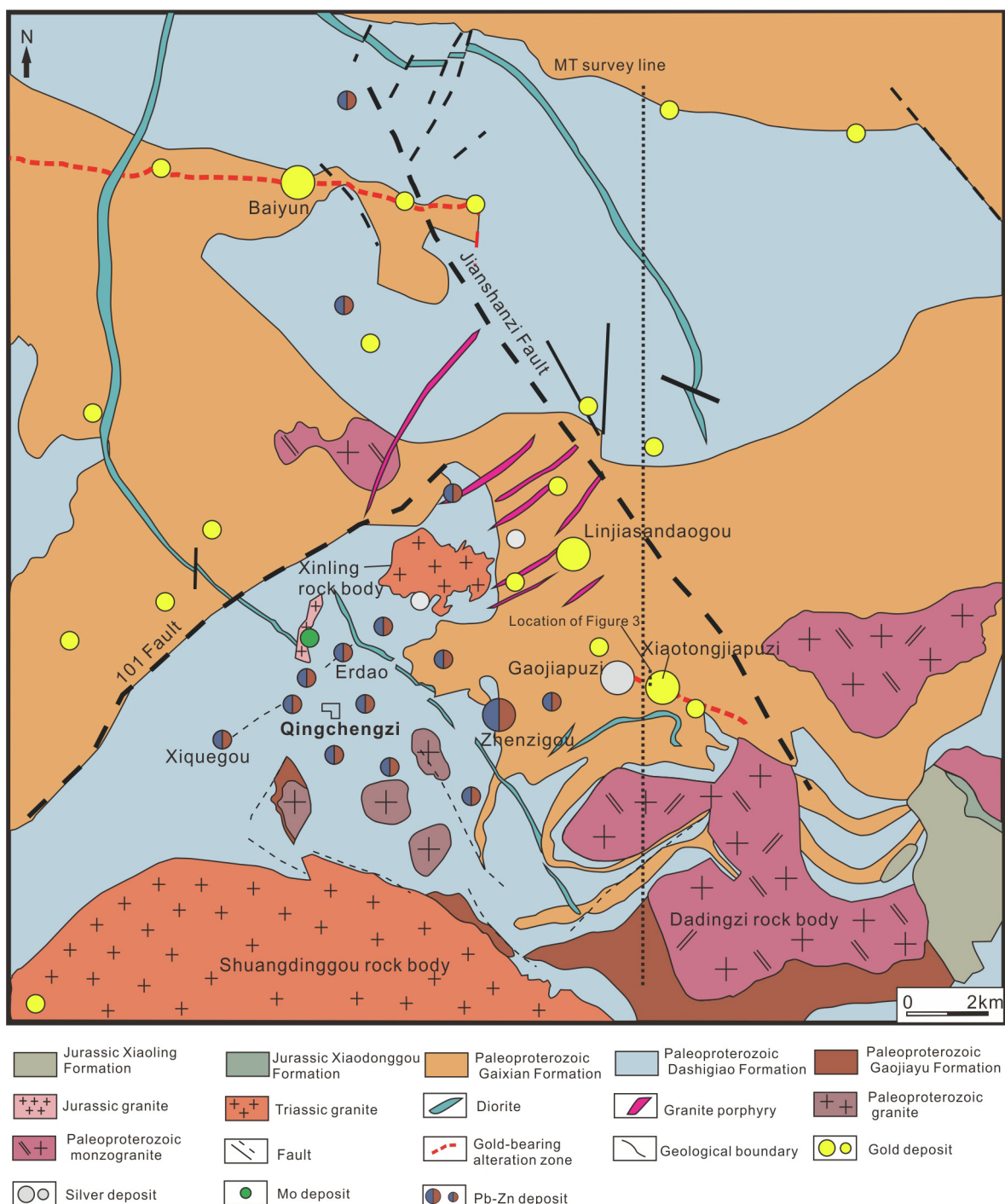


Fig. 2. Geological map of the Qingchengzi orefield. Locations of major gold deposits are illustrated with solid yellow circles (modified from Xiaoxia et al., 2017).

porphyry with an emplacement age of 225.3 ± 1.8 Ma (Gang Yu et al., 2009). The Yaojiagou intrusion consists of granite with zircon U-Pb age of 167.5 ± 0.9 Ma (Peng Zhang et al., 2016). Most of the dikes formed during the Triassic (Xiaoxia Duan et al., 2014), and some intermediate-acid dikes were emplaced in the Early Cretaceous (Sun et al., 2019a). The main structures in the Qingchengzi orefield are characterized by two main faults: NW-SE striking Jianshanzi fault and NE-SW striking 101 fault. Quite a few gold deposits occur along these two main faults and their secondary faults (Fig. 2). Some of the gold deposits developed at great depth within the fault system, and some as thick as 133.6 m, with a grade of 0.1–0.5 g/t or even up to 2.7 g/t in some locations.

The gold deposits in the Qingchengzi orefield consist of the

Xiaotongjiapuzi, the Linjiasandaogou, the Baiyun, the Yangshu, the Taoyuan, and a series of gold occurrences (Fig. 2). The gold deposits in this area are mainly distributed in three NW-trending belts: the Xiaotongjiapuzi, the Baiyun, and the Linjiasandaogou. The mineralization type is mostly the altered-rock type, with a small amount of quartz vein mineralization. Because the gold deposits share similar geological characteristics, we take the Xiaotongjiapuzi gold deposit as an example to illustrate their characteristics. The gold-bearing rocks are biotite granulite, marble, and schist at the top of Dashiqiao Formation in the Liaohe Group.

The orebodies are buried at a depth of 200 m below the surface, and are controlled by a local fractured zone, as demonstrated in the Fig. 3.

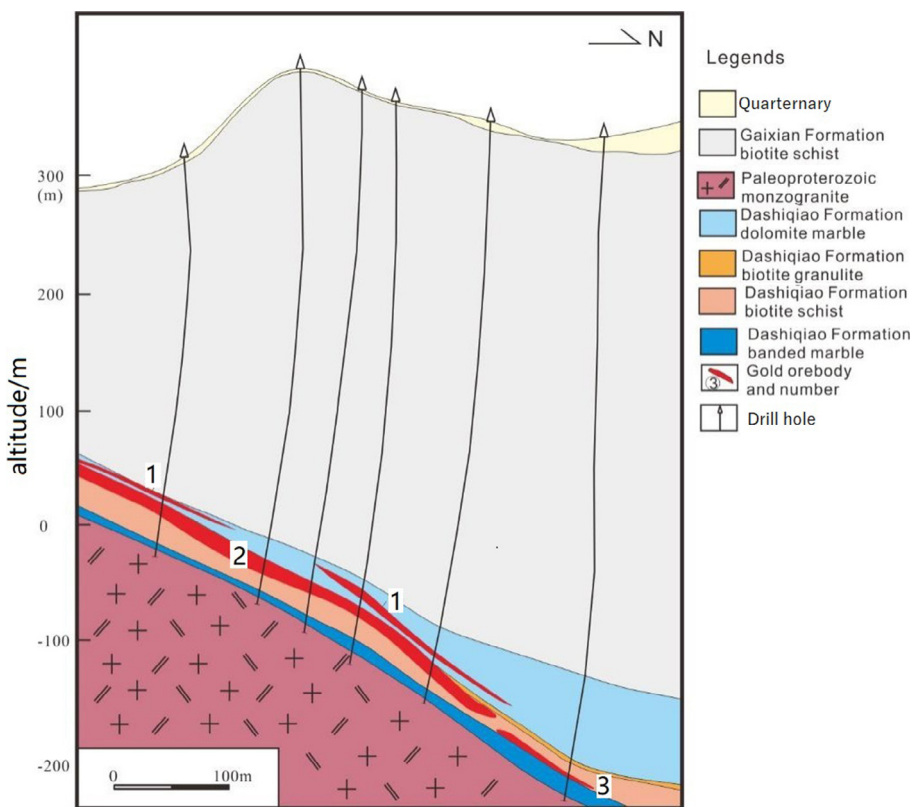


Fig. 3. Cross-section of the geological map for the Xiaotongjiapuzi gold deposit. The gold deposits are located in the fracture zone of the fault.

The ore-bearing layer is about 50–100 m thick and consists of three orebodies. The No. 1 orebody is located in the contact zone between the schist of the Gaixian Formation and the marble of the Dashiqiao Formation. The No. 2 orebody is located in the transition zone between the schist and the marble at the top of the Dashiqiao Formation. The No. 3 orebody is in the transition zone between the mica schist and the marble. The No. 1 orebody, which extends 500 m long and 200–600 m deep, is controlled by an east-westward, northeast-dipping (with a dip angle of 25°) fault. The No. 2 orebody, which extends 600 m long and 200 m deep, is controlled by a fracture with a strike of 285° and a dip angle of 25° (northeast-dipping). The No. 3 orebody is also controlled by a nearly east-westward and northeast dipping fracture and extends ~1000 m along the striking and 500 m deep, with a width of 2–10 m. The ore structures include stratified, banded, vein, disseminated, and breccia. Alteration types that include silicification, sericitization, pyritization, and carbonation are well developed (Limin Sun et al., 1997; Hongxia Liu et al., 2006). The most sulfide minerals are pyrite and arsenopyrite, which are also the uppermost gold-bearing minerals in the Xiaotongjiapuzi gold deposit.

Previous studies on H-O isotopes and ore-forming fluids demonstrate that the gold deposits in this area are post-magmatic hydrothermal deposits related to Mesozoic magmatic activities (Sen et al., 2012; Libo Hao et al., 2017; Fengchao Yang et al., 2016, 2017; Sun et al., 2019a,b). The deposits are controlled by faults and characterized by strong silicification and sericitization. The gold-bearing hydrothermal fluids from deeper part migrate upward through fractures in the fault zones. Pressure and temperature decreased where the faults become wider in the shallow part, resulting in precipitation of metallic minerals to form orebodies (Fig. 4). As illustrated in the geological model in the Fig. 4, gold orebodies have been found at shallow part (~1000 m) where the fault is relatively steep. Gold orebodies might also occur in the deep portion of the fault where its dip angle increases.

3. The SEP system

The SEP system was invented by the Institute of Geology and Geophysics, Chinese Academy of Sciences, for electromagnetic geophysical prospecting. It consists of a high-powered transmitter, distributed-structure receiver, electrical field sensors, induction coil magnetic sensors, and data processing and interpretation software. The system supports all common electromagnetic surveys, such as MT, audio-frequency magnetotellurics (AMT), controlled-source audio-frequency magnetotellurics (CSAMT), induced polarization, and wireless electromagnetic surveys. Table 1 presents some parameters of the SEP system.

The advantages of the portable transmitter are that it has a small volume and weight, which is key in mountainous terrain, and that it could also produce a high signal-to-noise-ratio signal with precise synchronization in a wide voltage range (Yiming Zhang and Ketang Hu, 2011). The distributed structure design is implemented in the portable receiver to enable very low power consumption. The receiver simultaneously records multiple electromagnetic signals via multiple channels, with great flexibility and user-friendly operation. The SEP system supports reliable three-dimensional (3-D) data acquisition of MT, AMT, and CSAMT surveys. We conducted several tests for the newly developed SEP system to evaluate and compare its performance with that of the aforementioned commercial electromagnetic instruments at test sites with different environmental conditions and terrains (Wanhua Zhu et al., 2013). We performed a comprehensive CSAMT study in the Jinchuan Ni-orefield, Gansun Province, Northwest China, and compared SEP performance (Qingyun Di, 2015), with MTU-RT, the GDP-32, and EH4 systems. We also completed an MT comparison study in the Caosiyao Mo deposit, Inner Mongolia, North China (Qingyun Di et al., 2015). These studies have demonstrated the reliability and flexibility of the SEP system.

We used the new version of the DRU receiver system for MT data acquisition. Fig. 5 presents the photographs of the receiver and

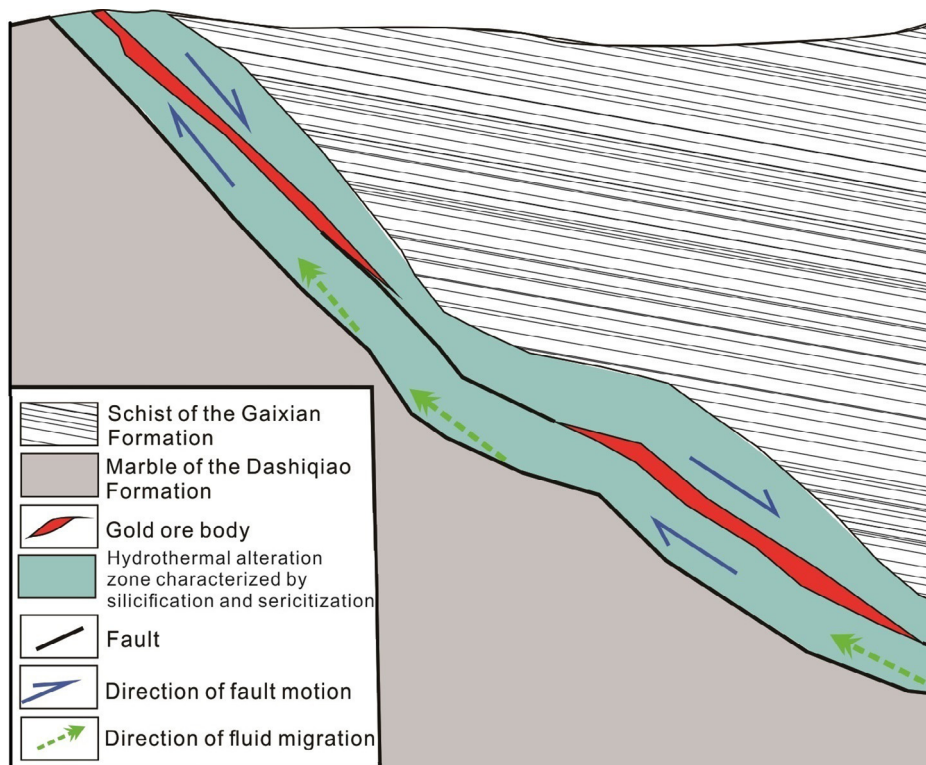


Fig. 4. A sketch of the mechanism by which the mineral deposits form. The gold-bearing hydrothermal fluids migrate upward along the fracture zone of the normal fault, precipitating metallic minerals as pressure and temperatures decrease, which usually occurs where the fault becomes deeper and wider.

Table 1
Parameters of the SEP system.

Magnetic sensor	Frequency band	10000 s–10 kHz
	Noise level	0.05pT/√Hz @ 1 Hz 0.5pT/√Hz @ 0.1 Hz
Receiver	Number of channels	12
	Dynamic range	≥130 dB
	Maximum sampling rate	48 kHz
	Power	1 W/channel
	Function	WEM, AMT, MT, CSAMT, IP
Transmitter	Power	≥50 kW
	Frequency band	Encodable

magnetic sensor. The induction-coil sensor has a noise level of $0.05\text{pT}/\sqrt{\text{Hz}}@1\text{ Hz}$ and a wide frequency band of $10,000\text{ Hz} \sim 10,000\text{ s}$. The noise level for the receiver is $0.6\mu\text{VRMS}@150\text{ Hz}$, and its frequency band and dynamic range are $\text{DC} \sim 10\text{ kHz}$ and $\geq 130\text{ dB}$, respectively. The receiver and sensors' low noise level and wide frequency band

enabled us to pick up the weak electromagnetic signal induced by the deeply buried targets in the noisy environment of the orefield.

In the MT measurement mode, three magnetic coils and two electric dipoles are setup for field measurement, which acquires the electric and magnetic components in 3 frequency bands (2.4 kHz, 150 Hz, and 15 Hz, respectively). The measuring time is set according to the required measurement depth. The phase value, apparent resistivity value and impedance are estimated using preprocessing software, and are used to obtain the underground information. **Fig. 6** presents the results of data quality control obtained by comparing the apparent resistivity of different sensors.

4. The MT survey and results

We performed a full 3-D MT survey and recorded the tensor field data, that is, the three magnetic fields components (H_x , H_y , and H_z) and the two horizontal electrical components (E_x and E_y). The sampling rates used were 2.4 kHz, 150 Hz, and 15 Hz, depending on the frequency band of interest and the buried depth of potential targets.

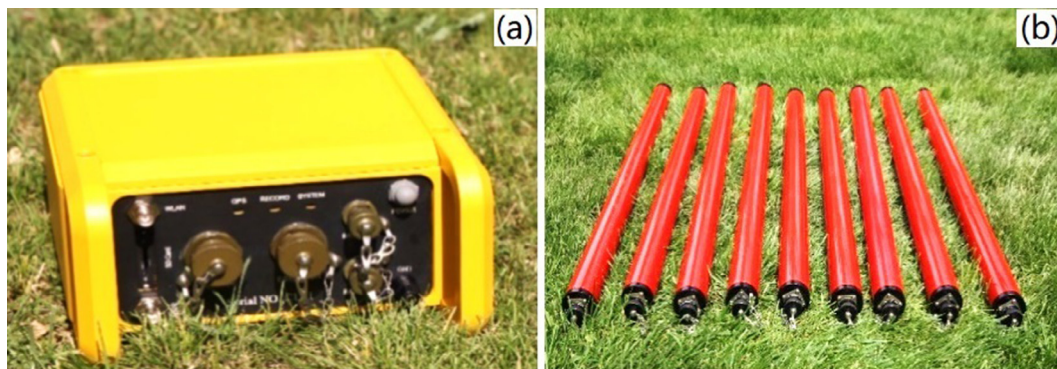


Fig. 5. Equipment used in this study. a) depicts the DRU broadband receiver; b) depicts the induction-coil magnetic sensor.

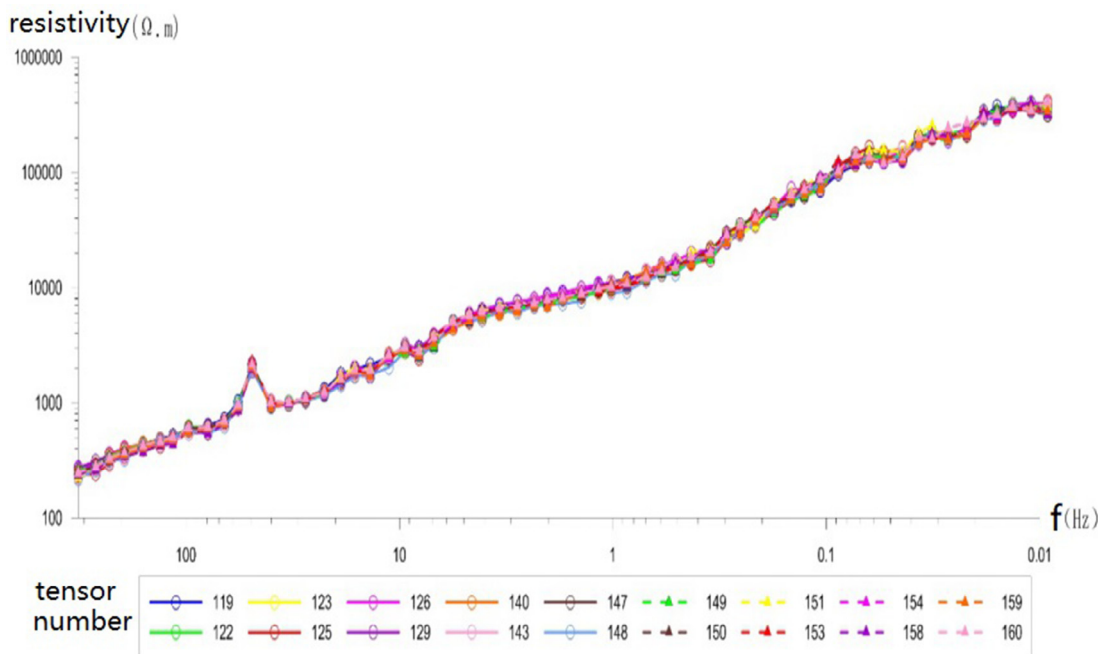


Fig. 6. Conformity measurement curve. In total, 18 sensors were tested (results indicated with different colors).

Impedance tensor and apparent resistivity were calculated from the tensor electromagnetic field data.

The data was denoised and filtered, and terrain effect on the data was mitigated by projecting the electrical field onto the horizontal plane. We applied two-dimensional (2-D) inversions to the data to obtain subsurface resistivity models (Routh and Oldenburg, 1999). The MT data inversion was conducted with WinGLink visualization integrated software, and the nonlinear conjugate gradient method (Rodri and Mackie, 2001) was selected for optimization. We discretized the 2-D inversion domain into 175*72 rectangular cells, and a homogeneous half-space of 100 O*m was selected as the initial model. The threshold error of TM mode data was set as 5% for both the resistivity and the impedance phase. To select an optimal regularization factor balancing model smoothness and data fitting, we ran several inversions with regularization factors between 0.1 and 100. Consequently, the inversion result with a regularization factor of 10 was selected, as it predicts the data well with an RMS error of 2.01 and is sufficiently smoothed. Fig. 7 provides a vertical section of the resistivity model.

The resistivity model, as demonstrated in the Fig. 7, is dominated by a low resistivity background, which we interpret to be the schist of Gaixian Formation. The high resistivity anomalies are interpreted to be the granite. The fault lies in the transition zone between the high- and low-resistivity areas. The interpreted position of the Jianshanzi fault, marked with the black dashed line in Fig. 7, indicates a northward inclination with a dip angle of about 75°. This intersects the survey line at Taoyuan, and was confirmed by known geology. The fault likely extends to a depth of more than 5 km, according to the resistivity model. The low resistivity on the southern portion of the cross-section is interpreted to be fracture zones associated with the northwestward Qingchengzi fault.

The survey line runs through two known gold deposits: the Xiaotongjiapuzi and Taoyuan gold deposits. The Taoyuan gold deposit is known to lie in the fracture zones between the Gaixian Formation and the Dashiqiao Formation and to likely be multi-layered. It inclines to the NE or NNE, with the same dip angle of ~25°. The location of the Taoyuan gold deposit is illustrated by magenta ellipses in Fig. 7, which coincides with a shallow low-to-high-resistivity transition zone. The transition zone extends to a significant depth of more than 2 km, indicating the possibility of potential deposits at a significant depth,

which should be examined by further studies. The Xiaotongjiapuzi gold deposit, marked by magenta ellipses in Fig. 7, is also in a low-to-high-resistivity transition zone. This transition zone also extends to a significant depth, suggesting potential deeply buried gold deposits. We present the interpreted location of potential gold deposits with red ellipses in Fig. 7.

5. Conclusions and recommendations

Several factors such as insufficient funding for mineral prospecting, biased models for predicting mineral resources, and limited coverage of geophysical surveys, resulted in little progress in gold prospecting in the Liaodong area. We have conducted a full 3-D MT survey in the Qingchengzi orefield in the Dandong area, Liaoning province, as well as have obtained a subsurface geoelectrical model of the survey area. The model is petrophysical and interpreted based on known geology in the survey area, and the interpreted results are partially confirmed by known geological information at shallow depth. Our high-resolution model provides detailed information on the location and geometry of the fault and the intrusive bodies. Our results suggest there may be gold orebodies present at greater depths, and helped us to predict their possible locations and dimensions. Our results support the hypothesis that the polymetallic deposit is a craton destruction-related post-magmatic hydrothermal type. This geophysical evidence further highlights the possibility of regional applications of the craton destruction-related post-magmatic hydrothermal model for predicting mineral resources in the Liaodong area.

Our study also serves as a new workflow model for mineral prospecting by successfully integrating a reasonable model for predicting the location and extent of mineral deposits from regional geological study, and new geophysical methods and instruments. These enable high-resolution deep earth exploration, and comprehensive petrophysical interpretation, incorporating known related geological information. Our study demonstrates that the integration of new geological, geophysical, and mineralogical tools and information could breed breakthroughs for mineral prospecting.

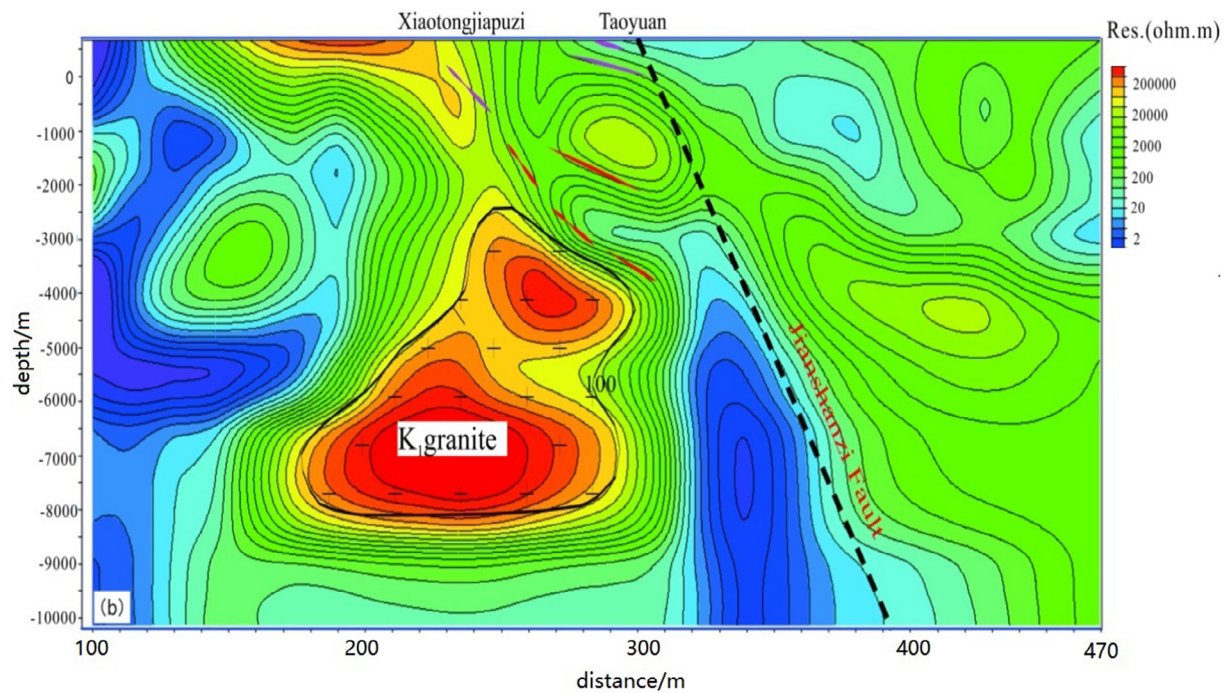


Fig. 7. Cross-section of the resistivity model. The black dashed line denotes the interpreted position for the Jianshanzi fault. The high-resistivity body is interpreted to be the K1 granite stock. The gold deposits should lie in the transition zone between the intrusive rock (presented as high-resistivity) and the country rock (presented as low-resistivity).

Acknowledgements

We acknowledge all of our colleagues participating in the development and testing of the SEP system. We also thank the technicians and engineers from Xi'an Northwest Nonferrous Metallic Geophysical and Geochemical Exploration Corps Co., Ltd., for helping with the MT data acquisition.

This research was supported by the National Key Research and Development Program of China (2016YFC0600101, 2017YFC0601204, 2018YFC0603200) and the Natural Science Foundation of China (NSFC) (41830101, 41874088).

Appendix A. Supplementary data

Supplementary data to this article can be found online at <https://doi.org/10.1016/j.oregeorev.2020.103501>.

References

- BGMELP (Bureau of Geology and Mineral Exploration of the Liaoning Province), 1989. Regional Geology of Liaoning Province. Beijing: Geological Publishing House p, 1–856 (in Chinese with English abstract).
- Qingyun, Di, Miaoyue, Wang, Kunfa, Shi, Gengli, Zhang, 2002. An applied study on prevention of water bursting disaster in mines with the high resolution V6 system. Chin. J. Geophys. 45, 05744–05748.
- Qingyun, Di, Guangjie, Wang, Zhiguo, An, Fei, Gong, Kunfa, Shi, Yingxian, Li, Ruo, Wang, Miaoyue, Wang, 2006. Geophysical exploration over long deep shield tunnel for the west route project of diverging water from Yangtze River to Yellow River. Chin. J. Geophys. 49 (6), 1836–1842.
- Qingyun, Di, Cheng, Xu, Changmin, Fu, Zhongxing, Wang, Wenxiu, Zhang, Zhiguo, An, Ruo, Wang, 2015. Surface Electromagnetic Prospecting System(SEP)contrast test in Caosiyuan molybdenum mine, inner mongolia. Chin. J. Geophys. 58 (8), 2654–2663.
- Qingyun, Di, 2015. Surface electromagnetic prospecting system (SEP) comparative test on Jinchuan nickel mine of Gansu Province. Chin. J. Geophys. 58 (10), 3845–3854.
- Qingyun, Di, Guangyou, Fang, Yiming, Zhang, 2013. Research of the Surface Electromagnetic Prospecting (SEP) System. Chin. J. Geophys. 56 (11), 3629–3639.
- Qingyun, Di, Changchun, Yang, Rixiang, Zh.u., 2012. Key technology development of deep resources exploration and field experimentation. Bull. Chin. Acad. Sci. 27 (3), 389–394.
- Zuquan, Du, Fuxing, Liu, Xigang, Wu., 2008. Analysis on geological characteristics and origin of Linjiasandaogou gold deposit. Gold 29 (4), 18–20.
- Xiaoxia, Duan, Qingdong, Zeng, Jinhui, Yang, Jianming, Liu, Yongbin, Wang, Lingli, Zhou, 2014. Geochronology, geochemistry and Hf isotope of Late Triassic magmatic rocks of Qingchengzi district in Liaodong peninsula, Northeast China. J. Asian Earth Sci. 91 (2014), 107–124.
- Xiaoxia, Duan, Qingdong, Zeng, Yongbin, Wang, Lingli, Zhou, Bin, Chen, 2017. Genesis of the Pb-Zn deposits of the Qingchengzi orefield, eastern Liaoning, China: Constraints from carbonate LA-ICPMS trace element analysis and C-O-S-Pb isotopes. Ore Geol. Rev. 89, 752–771.
- Libo, Hao, Xin, Zhao, Yuyan, Zhao, 2017. Stable isotope characteristics and ore genesis of the Baiyun gold deposit, Liaoning Province. J. Jilin Univers. (Earth Sci. Ed.) 47 (2), 442–451 (in Chinese with English abstract).
- Guoping, Liu, Yongfu, Ai, 2002. Study on ore-forming epoch of Xiaotongjiapuzi gold deposit, Liaoning Province. Mineral Depos. 21 (1), 53–59 (in Chinese with English abstract).
- Hongxia, Liu, Hanquan, Kong, Yanchen, Yang, 2006. Geologic characteristics and genesis of Xiaotongjiapuzi gold deposit, Liaoning Province. Gold 27 (5), 13–16 (in Chinese with English abstract).
- Jun, Liu, Fuxing, Liu, Senghui, Li, Kit, Lai, 2019. Formation of the Baiyun gold deposit, Liaodong gold province, NE China: Constraints from zircon U-Pb age, fluid inclusion, and C-H-O-Pb-He isotopes. Ore Geol. Rev. 104, 686–706.
- Rodi, W., Mackie, R.L., 2001. Nonlinear conjugate gradients algorithm for 2D magnetotelluric inversion. Geophysics 66 (1), 174–187.
- Routh, P.S., Oldenburg, D.W., 1999. Inversion of controlled source audio-frequency magnetotellurics data for a horizontally layered earth. Geophysics 64 (12), 1689–1697.
- Yunhong, Song, Fengchao, Yang, Guolei, Yan, Minghui, Wei, Shaoshan, Shi, 2016. SHRIMP U-Pb ages and Hf isotopic compositions of Paleoproterozoic granites from the eastern part of Liaoning Province and their tectonic significance. Acta Geol. Sin. 90 (10), 2620–2636 (in Chinese with English abstract).
- Limin, Sun, Wentao, Sun, Guangfan, Zhao, 1997. Geological characteristics of Xiaotongjiapuzi gold-silver deposit of Qingchengzi orefield and its source of mineralized matter. Gold 18 (12), 13–18 (in Chinese with English abstract).
- Weidong, Sun, 2015. Decratonic gold deposits: a new concept and new opportunities. Natl. Sci. Rev. 2 (3), 248–252.
- Sun, G.T., Zeng, Q.D., Wang, Y.B., Li, B., Chen, P.W., 2019a. Geochronology and geochemistry of Mesozoic dykes in the Qingchengzi ore field, Liaoning Province, China: Magmatic evolution and implications for ore genesis. Geol. J. <https://doi.org/10.1002/gj.3646>.
- Sun, G.T., Zeng, Q.D., Li, T.Y., Li, A., Wang, E.Y., Xiang, C.S., Wang, Y.B., Chen, P.W., Yu, B., Wang, R.L., 2019b. Ore genesis of the Baiyun gold deposit in Liaoning province, NE China: constraints from mineralogy, fluid inclusions, and zircon U-Pb ages. Arabian J. Geosci. 2019. <https://doi.org/10.1007/s12517-019-4459-0>.
- Yuwang, Wang, Hongjin, Xie, Dedong, Li, Shi, Yu, Fuxing, Liu, Guoqiang, Sun, Qiming, Sun, Guochao, Zhou, 2017. Prospecting prediction of ore concentration area exemplified by Qingchengzi Pb-Zn-Au-Ag ore concentration area, eastern Liaoning Province. Mineral Depos. 36 (1), 1–24 (in Chinese with English abstract).
- Fengchao, Yang, Yunhong, Song, Peng, Zhang, Peng, Chai, Bin, Li, 2016. Forming fluid

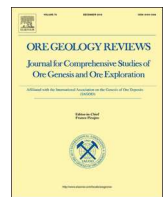
- characteristics and tracing of ore-forming sources materials of gold-silver deposit in the Qingchengzi ore concentration area. *Acta Geol. Sin.* 90 (10), 2775–2785 (in Chinese with English abstract).
- Fengchao, Yang, Yunhong, Song, Peng, Chai, Bin, Li, 2017. Characteristics of ore-forming fluid and provenance of ore-forming material of Baiyun gold deposit in Liaoning. *J. Mineral. Petrol.* 37 (1), 30–39 (in Chinese with English abstract).
- Gang, Yu., Jiangfeng, Chen, Chunji, Xue, 2009. Geochronological framework and Pb, Sr isotope geochemistry of the Qingchengzi Pb-Zn-Ag-Au orefield, Northeastern China. *Ore Geol. Rev.* 35, 367–382.
- Bin, Yu., Qingdong, Zeng, Yongbin, Wang, Weikang, Guo, Guotao, Sun, Tianchen, Zhou, Jianping, Li, 2018. Genesis of the Wulong gold deposit, northeastern North China Craton: constraints from fluid inclusions, S-Pb isotopes and pyrite LA-ICPMS trace element analysis. *Ore Geol. Rev.* 102, 313–337.
- Qingdong, Zeng, Renyi, Chen, Jinhui, Yang, Sun Guotao, Yu, Bing, Wang Yongbin, Peiwen, Chen, 2019. The metallogenetic characteristics and exploring ore potential of the gold deposits in eastern Liaoning Province. *Acta Petrol. Sin.* 35 (7), 1939–1963 (in Chinese with English abstract).
- Mingguo, Zhai, Jinhui, Yang, Hongrui, Fan, Laicheng, Miao, Yonggang, Li, 2002. A large-scale cluster of gold deposits and metallogenesis in the Eastern North China Craton. *Int. Geol. Rev.* 44 (5), 458–476.
- Lianchang, Zhang, Yang, Bai, Mingtian, Zh.u., Ke, Huang, 2018. Regional differences of gold deposits on the North China Craton. *J. Earth Sci. Environ.* 40 (4), 363–380 (in Chinese with English abstract).
- Sen, Zhang, Di, Zhang, Dexi, Sh.a., Linlin, Kou, Dongfang, Zhao, 2012. Metallogenetic characteristics and genesis of the gold (silver) mineralization in Linjiasandaogou-Xiaotongjiapuzi area, eastern Liaoning Province. *J. Jilin Univ. (Earth Sci. Ed.)* 42 (3), 725–732 (in Chinese with English abstract).
- Peng, Zhang, Hongzhi, Yang, Bin, Li, Leilei, Kou, Feichao, Yang, 2016. Ore source, ore-forming age and geodynamic setting of Yaojiagou molybdenum deposit in Qingchengzi ore-clustered area, Eastern Liaoning Province. *J. Jilin Univ. (Earth Sci. Ed.)* 46 (6), 1684–1696 (in Chinese with English abstract).
- Zhang Yiming and Hu Ketang. 2011. Powerful transmitter structure with wide-range continuously adjustable output voltage. The utility model patent ZL201110216984.3.
- Wanhua, Zhu, Qingsun, Di, Leisong, Liu, Bin, Yan, Kai, Liu, Guangyou, Fang, 2013. Development of search coil magnetometer based on magnetic flux negative feedback structure. *Chin. J. Geophys.* 56 (11), 3683–3689.
- Rixiang, Zh.u., Hongrui, Fan, Li, J.W., Meng, Q.R., Li, S.L., Zeng, Q.D., 2015. Decratonic gold deposits. *Sci. China Earth Sci.* 58 (58), 1523–1537.

Update

Ore Geology Reviews

Volume 124, Issue , September 2020, Page

DOI: <https://doi.org/10.1016/j.oregeorev.2020.103635>



Corrigendum to “Magnetotelluric exploration of deep-seated gold deposits in the Qingchengzi orefield, Eastern Liaoning (China), using a SEP system” [Ore Geol. Rev. 122 (2020) 103501]



Qingyun Di^{a,b,d,e}, Guoqiang Xue^{c,d,e,*}, Qingdong Zeng^{c,d,e}, Zhongxing Wang^{a,b,d,e}, Zhiguo An^{a,b,d,e}, Da lei^{a,b,d,e}

^a Key Laboratory of Shale Gas and Geoengineering, Institute of Geology and Geophysics, Chinese Academy of Sciences, Beijing 100029, China

^b Frontier Technology and Equipment Development Center for Deep Resources Exploration, Institute of Geology and Geophysics, Chinese Academy of Sciences, Beijing 100029, China

^c Key Laboratory of Mineral Resources, Institute of Geology and Geophysics, Chinese Academy of Sciences, Beijing 100029, China

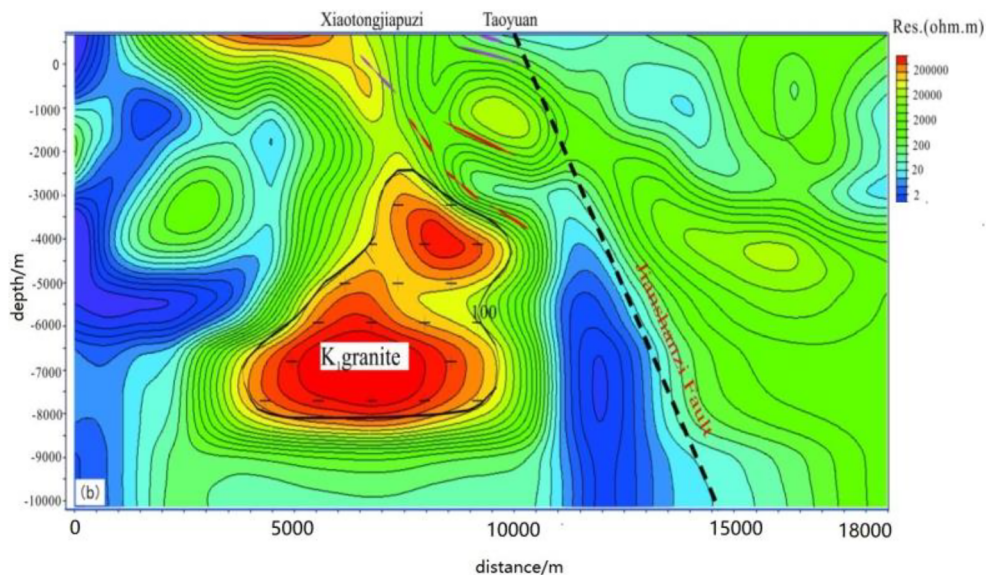
^d College of Earth and Planetary Sciences, University of Chinese Academy of Sciences, Beijing 100049, China

^e Innovation Academy for Earth Science, Chinese Academy of Sciences, Beijing, 100029, China

The authors regret to inform that the label of Fig. 7 was erroneous in the article. More specifically, the horizontal label that was 100 to 470 m should range from 0 to 18000 m. The correct Fig. 3 is as follows:

In addition, the authors inform that the following yellow color marked words is correct. “We discretized the 2-D inversion domain into 175 * 72 m rectangular cells, and a homogeneous half-space of 100 Ω·m was selected as the initial model.”

The authors informs that the following yellow color marked words is correct. “Our results suggest there may be gold orebodies present at



DOI of original article: <https://doi.org/10.1016/j.oregeorev.2020.103501>

* Corresponding author.

E-mail address: ppxueguoqiang@163.com (G. Xue).

greater depths, and helped us to predict their locations and dimensions.”

The authors regret to inform “Whilst the Jianshanzi fault zone (Fig. 2) is known to be gold-mineralized to depths of approximately 420 m it is not known whether the gold orebody has potential to extend deep underground and whether further orebodies may occur within 3000 m depth “(where, “420 m it” should become as “420 m it”, “3000 m depth”) should be changed as “3000 m depth”.

The authors regret to inform “Fig. 6. Conformity measurement curve. In total, 18 sensors were tested (results indicated with different colors), should be changed as Fig. 6. Conformity measurement curve. In total, 18 sensors were tested (results indicated with different colors)”.

The authors would like to apologise for any inconvenience caused.